Journal of Photonics for Energy

PhotonicsforEnergy.SPIEDigitalLibrary.org

Review on methods for improving the thermal and ambient stability of perovskite solar cells

Yuxiong Zhou
Jinghua Hu
Yuxia Wu
Rongbang Qing
Chengming Zhang
Xiaoying Xu
Minlin Jiang

SPIE.

Yuxiong Zhou, Jinghua Hu, Yuxia Wu, Rongbang Qing, Chengming Zhang, Xiaoying Xu, Minlin Jiang, "Review on methods for improving the thermal and ambient stability of perovskite solar cells," *J. Photon. Energy* **9**(4), 040901 (2019), doi: 10.1117/1.JPE.9.040901.

REVIEW

Review on methods for improving the thermal and ambient stability of perovskite solar cells

Yuxiong Zhou,[a,†] Jinghua Hu,[a,†] Yuxia Wu,[b] Rongbang Qing,[a] Chengming Zhang,[a] Xiaoying Xu,[a,*] and Minlin Jiang[b,*]

[a]Wuhan University of Technology, Department of Physics, Wuhan, Hubei, China
[b]Nanchang University, Institute of Advanced Study, Nanchang, Jiangxi, China

Abstract. Perovskite solar cells (PSCs) are solar cells that are efficient, low cost, and simple to fabricate. Over the last 9 years, researchers have conducted in-depth research on PSCs to increase their photoelectric conversion efficiency from 3.8% to 24.2%. PSCs have the potential to replace traditional energy sources in the future. However, the stability of these cells is poor, which limits their practical applications, because the perovskite material is susceptible to degradation by environmental factors, such as moisture, heat, and oxygen. In our review, some studies related to improving the stability of PSCs are summarized. Strategies that have been developed to improve the stability of PSCs are reviewed from the aspects of the electron transport, perovskite, and hole transport layers (HTLs). These strategies include doping the electron transport layer (ETL), using dopant-free HTL, grain passivation, employing double layers or graded hybrid structure of ETL or HTL, two-dimensional perovskites, and so on. We provide a reference for future studies on the stability of PSCs. [DOI: 10.1117/1.JPE.9.040901]

Keywords: perovskite solar cells; stability; review.

Paper 19077MV received Aug. 17, 2019; accepted for publication Dec. 3, 2019; published online Dec. 18, 2019.

1 Introduction

Fossil energy cannot meet future demands, on account of the depletion of the necessary resources and the accompanying environmental problems. Therefore, researchers have exerted efforts to convert clean solar energy into electricity via the photovoltaic effect. Over the last few years, Si, CdTe, CuInGa/Se, and other light-absorbing materials have been employed to fabricate solar cells. However, the effects of these materials are not ideal. Then, researchers found a new light-absorbing material, the perovskite material.

The molecular formula of perovskite is ABX_3 [Fig. 1(a)]; here, A is a monovalent cation, B is a divalent metal cation, and X is a halogen anion. Kojima et al.[1] fabricated perovskite solar cells (PSCs) for the first time by using the perovskite material $CH_3NH_3PbI_3$ ($MAPbI_3$) as a light-absorbing material in dye-sensitized solar cells; the power conversion efficiency (PCE) of these cells was 3.8%. The excellent photovoltaic performance of PSCs attracted the attention of researchers worldwide. Indeed, in just a few years, the conversion efficiency of these cells has been rapidly improved from 3.8% to 24.2%,[2] which indicates that PSCs with a layered structure may become a new energy source in the future. Figure 1(b) shows a schematic of a planar heterojunction PSC.

Despite their many benefits, however, PSCs present serious stability problems and have a short effective life, mainly because the perovskite material is susceptible to environmental factors, such as oxygen, moisture, thermal stress,[3,4] light, and applied electric fields.[5] These factors lead to material degradation, resulting in a short cell life.[6] Furthermore, a large number of defect states are observed in PSCs, and these states can not only affect the photoelectric performance of a PSC but also damage its stability.

*Address all correspondence to Xiaoying Xu, E-mail: xu_xiao_ying@126.com; Minlin Jiang, E-mail: semiflyer1978@hotmail.com
†Yuxiong Zhou and Jinghua Hu contributed equally to this work.

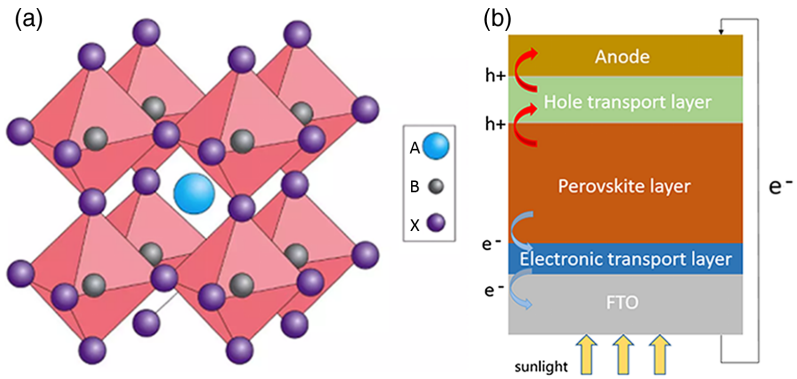

Fig. 1 Schematic diagram of (a) the atomic structure of perovskite crystals and (b) a planar heterojunction PSC.

Direct contact with the external environment can easily lead to the degradation of a PSC. Diverse encapsulation method[7,8] of PSCs can prevent the influence of the external environment to a certain extent, which helps to improve the stability of the PSC. Even if the cell is not encapsulated, there are many other ways to improve stability.

This paper reviews research on efforts to improve the stability of PSCs from three aspects, namely, the electron transport layer (ETL), perovskite layer, and hole transport layer (HTL). We assessed doping, substitution, composite structure methods, and two-dimensional (2-D) perovskites, which have been developed to improve the tolerance of PSCs to humidity, oxygen, and thermal stress. This discussion does not focus on other factors, such as light or applied electric fields, that contribute to the instability of perovskites.

2 Electronic Transport Layer

The ETL extracts electrons from the perovskite layer while preventing the reverse transport of holes and balancing electron–hole transport distances. In a planar heterojunction PSC, the ETL is also called the dense layer. Anatase TiO_2 is also the most commonly used electron transport material (ETM).

The characteristics of the ETM not only affect cell stability but are also closely related to the optoelectronic performance of the device. ETLs for high-performance PSCs usually have the following features: (1) high light transmittance to reduce light loss; (2) energy level matching, which can improve electron extraction efficiency and reduce energy loss; (3) simple preparation; (4) high electron mobility; (5) low trap state density; and (6) can prevent moisture and oxygen from entering the perovskite layer.

TiO_2 ETLs are used so that the resulting nanoTiO_2 is simple to prepare and has a suitable forbidden band width of 3.2 eV that can effectively suppress the reverse transport of holes. TiO_2 crystals fabricated via the conventional method exhibit high-electron trap state and poor photoelectric performance. The long-term stability of the device is not ideal because trivalent Ti ions and oxygen vacancies are generated by the irradiation of TiO_2 valence band electrons under ultraviolet (UV) light.[9] Oxygen vacancies on the surface of TiO_2 can adsorb oxygen and water molecules, thereby accelerating the degradation of the perovskite layer.

2.1 *Doping Method*

Pathak et al.[9] solved the problem of oxygen vacancies in TiO_2 dense layers by doping with trivalent metal cations. When the TiO_2 dense layer is prepared, the sol–gel method is carried out using a precursor mixture containing Ti and Al. As shown in Fig. 2, Al can be doped into the anatase lattice by substitution, thereby passivating electron defect sites and surface defects in the TiO_2 lattice. Al can also eliminate the sub-band gap state and increase the band gap to solve the stability problem caused by oxygen vacancies. The conductivity of Al is better than that of TiO_2, and a small amount of Al doping can improve the electron transport efficiency of the ETL.

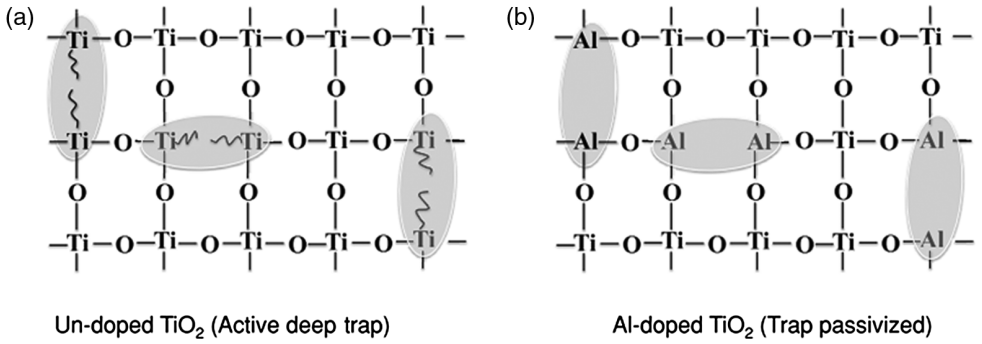

Fig. 2 Schematic of Ti(III) trap passivation, doping, and oxygen adsorption. (a) Oxygen defects in the crystal lattice cause Ti(III) defects, forming deep electron traps. (b) Al substitution of Ti(III) inactivates these defect sites.[9]

Yin et al.[10] successfully doped Nb into TiO_2 films via low-temperature solution treatment and obtained an efficient Nb-doped TiO_2 ETL with better conductivity and better electron mobility. The electron trap-state density of $CH_3NH_3PbI_3$ coated on TiO_2 is 1.63×10^{16} cm^{-3}. But that of $CH_3NH_3PbI_3$ deposited on 1% Nb-doped TiO_2 reduced to 1.13×10^{16} cm^{-3}. These led to an increase of PCE from 18.14% to 19.23% and a better stability against air and thermal. After storage for 1200 h in air, the PCE of the Nb-doped device remained at 90% of the initial PCE, whereas that of the pure TiO_2 device decreased to 67.6% of its initial value. In terms of thermal stability, the PCE of the Nb-doped TiO_2 device could maintain over 90% of its initial value after annealing for 20 h at 80°C in glove box. Under the same conditions, the PCE of the pure TiO_2 device rapidly decreased to 54% of its initial value. Peng et al.[11] prepared a high-quality In-doped Ti oxide ETL by using a simple one-step solution method. In-doping increased the electron conductivity of the layer and reduced the density of its sub-band gap state. Thus, the fill factor and open circuit voltage of the resulting perovskite cell were improved. Electron defects or trap states caused by oxygen defects in the TiO_2 lattice can be inactivated by In, which effectively improves the stability of the cell.

2.2 *Substitution Method*

An ideal ETM should have excellent optical properties and a suitable energy band while selectively extracting electrons and reducing recombination at the interface. To improve the stability of PSCs, besides TiO_2, other materials can be introduced as a charge transport material.

2.2.1 *Organic compounds*

A hydrophobic ETM can be introduced to improve the moisture resistance of perovskite devices without loss of photovoltaic performance. The most commonly used organic ETM is fullerene-derived phenyl-C_{61}-butyric acid methyl ester ($PC_{61}BM$). Fullerene C_{60} and $PC_{61}BM$ were first used by Jeng et al.[12] as ETMs in inverted-structured PSCs with a PCE of 3.9%. As the electron conductivity of $PC_{61}BM$ is higher than that of TiO_2, the former can improve the electron extraction from $MAPbI_3$ to the ETL. The corrosion-resistant architecture and hydrophobicity of $PC_{61}BM$ also improve air and humidity stability. The poor PCE observed is attributed to the thin perovskite absorbing layer of <100 nm, which limits the light harvesting and short-circuit current of devices. You et al.[13] and Docampo et al.[14] used a 300-nm-thick mixed halide–perovskite film and improved PCE to 11.5%. Heo et al.[15] used $PC_{61}BM$ as an ETL. They found that $PC_{61}BM$ could passivate the defects at the grain boundaries.

Li et al.[16] designed triphenylamine fullerene (TPA-PCBM) with a stronger charge transfer capability and higher carrier density compared with those of PCBM. A cross-linked silane functional fullerene ETL was designed by Bai et al.[17] to isolate moisture from PSCs. The unsealed C_{60}-SAM-based device maintained nearly 90% of its original efficiency after 30 days of exposure to the environment.

Metal oxides, such as ZnO, combined with fullerene as an ETL, improve the ohmic contact and device stability.[18] This improvement is described in detail in the following sections.

2.2.2 *Inorganic compounds*

Intrinsic oxygen vacancies on the TiO_2 surface are suspected to be among the main reasons behind the degradation of PSCs. Liu and Kelly[19] first used ZnO as a PSC ETL. ZnO has a similar energy level position and higher electron transport rate than TiO_2. The PCE of a cell fabricated with this material reached 15.7% under 1.5 AM sunlight irradiation. However, ZnO is very sensitive to weak bases or acids and has a high defect density. These characteristics result in serious electron hole recombination on the material surface, which is a factor of instability in PSCs.

Brinkmann et al.[18] introduced a bilayered electron extraction interlayer consisting of aluminum-doped zinc oxide (AZO) and SnO_x in inverted-structured PSC. As shown in Fig. 3, a PCBM layer is deposited on top of the $CH_3NH_3PbI_3$ perovskite layer. An AZO layer on $PC_{61}BM$ layer is derived from a nanoparticle dispersion, which is excellently suited to extract electrons from $PC_{61}BM$. An SnO_x layer with high electrical conductivity is deposited on top of the AZO layer by atomic layer deposition to form an outstandingly dense gas permeation barrier that effectively hinders the ingress of moisture toward the perovskite. At the same time, SnO_x can prevent the egress of decomposition products of the perovskite, which then corrode the metal electrodes and shorten the lifespan of cells. Consequently, the overall decomposition of perovskite is considerably suppressed, and the cells based on AZO/SnO_x do not degrade even after 300 h in ambient air (23°C and 50% RH). Yang et al.[20] complexed ethylenediaminetetraacetic acid (EDTA) with SnO_2 in planar-type PSCs to realize an EDTA-complexed SnO_2 (E-SnO_2) ETL. Its electron mobility is approximately three times larger than that of SnO_2. The PCE of the device with E-SnO_2 ETL increases to 21.60%. Moreover, the unencapsulated device based on E-SnO_2 maintains 92% of its initial efficiency exposed to an ambient atmosphere (35% RH) after 2880 h in the dark, whereas the device using only SnO_2 provides 74% of its initial efficiency under the same storage condition. In the continuous irradiation test, the device using the E-SnO_2 maintains 86% of its initial efficiency, whereas the device using only SnO_2 remains 38% relative to its initial efficiency after 120 h of illumination at 100 mW cm^{-2}.

Hwang and Yong[21] applied CdS as a new inorganic ETM to replace the traditional dense TiO_2 layer. CdS has a suitable conduction band energy level and no oxygen vacancy defects. Test results showed that the CdS-based PSC possesses significant light stability, and the resulting PCE retained over 90% of its initial value after 12 h of continuous standard 1.5 AM sunlight irradiation. By comparison, a TiO_2-based PSC retained only 18% of its initial PCE under the same conditions.

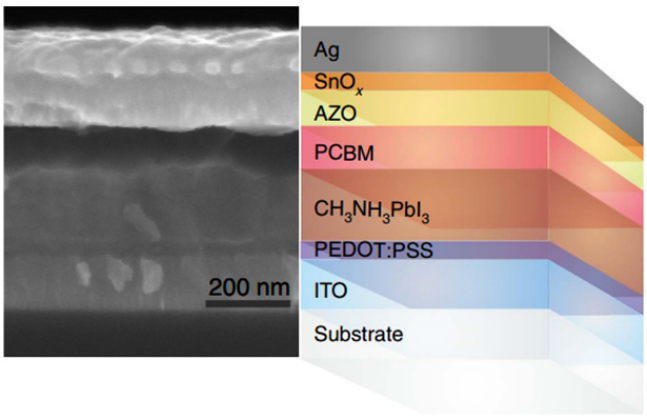

Fig. 3 Scanning electron microscopy image of the device cross-section along with the assignment of the respective layers.[18]

2.3 *Composite Structure Method*

2.3.1 *Two-layered structures*

A two-layered structure can be designed to synergize different ETMs, modify the contact between ETL/perovskite interfaces, and improve device stability. Qiu et al.[22] reported a $PC_{61}BM/ZnO$ double-layer ETL to improve the interface between this layer and the perovskite layer because the direct contact of $PC_{61}BM$ with a metal electrode is not conducive to electron extraction due to energy level mismatch. This issue can be addressed by inserting an additional layer of ZnO into the material. This ZnO layer not only improves the energy level matching of the device but also blocks the reaction between the metal electrode and the perovskite component that breaks down the perovskite structures. Moreover, the two-layered structure can protect the perovskite layer from air because of its barrier capability.

Singh and Nalwa[23–25] demonstrated that graphene-based materials can improve heterojunctions and enhance the stability of dye-sensitized photovoltaic devices. On the basis of Singh and Nalwa's work, Agresti et al.[26] used TiO_2/Li-modified graphene oxide (GO-Li) as a double-layer ETL. When the device was exposed to moisture, the GO-Li layer acted as a reaction center to prevent moisture infiltration. The GO-Li layer could also passivate the oxygen vacancies and defects of the mesoporous TiO_2 layer. Moreover, GO-Li and TiO_2 showed good energy matching, which improved the electron injection efficiency from the perovskite layer to the transport layer. The tested devices with double-layer ETL showed an improved stability when compared to the device with pure TiO_2 ETL in illumination aging test, but the physical mechanism of the improvement was not sure.

Song et al.[27] designed a two-layered ETL of SnO_2/TiO_2. The double-layered ETL had a larger contact area with the perovskite layer, a larger free energy difference, and suitable electron mobility. In addition, it allowed smooth contact with the FTO. The efficiency of a device fabricated with this layer was stable at 20.2% with almost no hysteresis behavior.

2.3.2 *Core/shell structures*

Surface trap sites could be improved by designing the ETL as a core/shell structure to increase stability. Hwang et al.[28] used core/shell-structured TiO_2/CdS as an ETL; here, the CdS coated on the TiO_2 layer surface inhibits the activation of oxygen vacancies in TiO_2, as shown in Fig. 4, and the CdS shell is effectively passivated by TiO_2 surface defects, thus preventing charges from recombining at the interface and oxygen from entering the perovskite. The resulting device maintained nearly 80% of its initial PCE after 12 h of continuous standard 1.5 AM sunlight exposure.

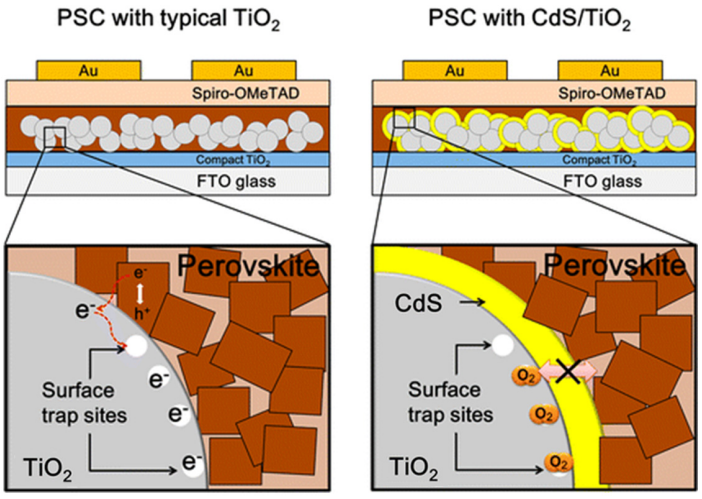

Fig. 4 Schematic of the mechanism of the CdS shell of the TiO_2 layer.[27]

3 Perovskite Layer

The stability of the perovskite layer is not only key to the long-term stability of PSCs but also affects their PCE. $MAPbI_3$ is the most commonly used perovskite material; it features high carrier mobility and strong light absorption. However, $MAPbI_3$ is also particularly sensitive to the external environment. The main factors affecting the instability of perovskite materials include the following:

1. Humidity.[29,30] $CH_3NH_3PbI_3$ is hygroscopic and eventually decomposes into CH_3NH_3I and PbI_2 when exposed to water.

$$CH_3NH_33PbI_3 \rightleftharpoons CH_3NH_3I + PbI_2$$

2. Thermal stress.[31,32] $CH_3NH_3PbI_3$ begins to decompose at 230°C.
3. Light and oxygen.[33–35] O_2 and UV light may accelerate perovskite degradation.
4. Applied electric fields (bias-dependent degradation).[36,37] Applied electric fields can also accelerate perovskite degradation. Accelerated degradation under open-circuit conditions is ascribed to trap charging combined with radical formation and assisted by undesirable extrinsic ion diffusion that is not prevented by internal fields. Slow degradation under short-circuit and maximum power-point conditions is attributed to internal and external ion migration due to internal interfacial fields.
5. Other factors.[34] As intrinsic elements of instability, the surface morphology, crystal phase transition, photo trap state, and grain boundary behavior of the material can also affect the stability of perovskite materials.

PSCs often exhibit reversible degradation processes because of light-soaking effect, thus leading to significant PCE variation during a day/night cycle. The PCE of some devices drops during the day but recovers during the night, but that of others exhibit the opposite. The reversible degradation mechanism poses new challenges for assessing the performance and lifespan of PSCs.[38] In this section, we focus on the improvement of the humidity and thermal stability of the perovskite layer. We do not discuss reversible degradation mechanisms or bias-dependent degradation of perovskites.

3.1 *Substitution Method*

Other ions could be used to completely or partially substitute atoms at the A, B, and X positions. In a crystal structure, the tolerance factor "t" is generally used as a metric to deviate from the ideal structure. For perovskite structures:

$$t = (R_A + R_X)/\sqrt{2}(R_B + R_X),$$

where R_A, R_B, and R_X are the ionic radii of the A, B, and X ions, respectively. The structural stability of perovskite can be reflected by t, and the basic structure of ABX_3 can be maintained in the range of $0.78 < t < 1.05$.[39] Several ions could be embedded in the photoactive perovskite phase by using various ion formulations, thereby improving the stability of the perovskite by regulating its crystal structure.

3.1.1 *Organic perovskites*

The first perovskite material used in the photovoltaic field is $MAPbI_3$. Methylamine (MA) is thermally unstable, whereas formamidine (FA) is relatively stable. The decomposition temperatures of $MAPbI_3$ and $FAPbI_3$ are 230°C and 290°C, respectively. Mei et al.[40] used 5-aninovaleric (5-AVA) to partially replace MA in $MAPbI_3$ in hole-conductor–free PSC. $(5\text{-AVA})_xMA_{1-x}PbI_3$ exhibited better stability under standard 1.5 AM sunlight in air. Compared with $MAPbI_3$, the $(5\text{-AVA})_xMA_{1-x}PbI_3$ perovskite layer showed better interfacial contact with TiO_2, which indicated a much lower defect concentration. Many studies have attempted the partial substitution of Br to form a MAPb $(I_{1-x}Br_x)_3$ material.[41,42] Because the substitution of larger I atoms with smaller Br atoms in $MAPb(I_{1-x}Br_x)_3$ leads to the reduction of

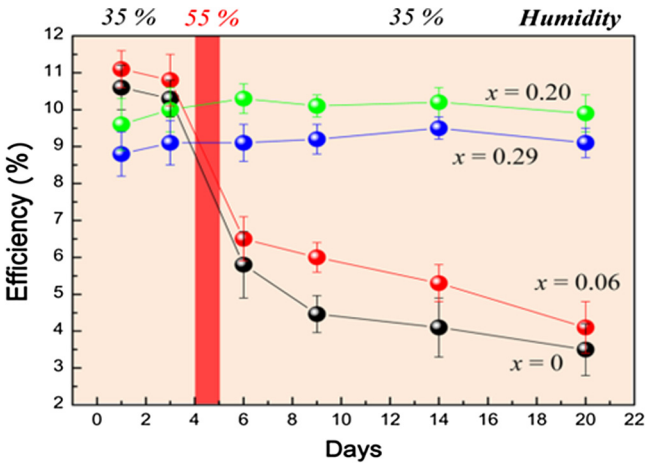

Fig. 5 Line graph of the PCE of heterojunction solar cells based on $MAPb(I_{1-x}Br_x)_3$ ($x = 0$, 0.06, 0.20, 0.29) versus time. Cells were exposed to 55% humidity on the fourth day and maintained at 35% RH for the rest of the experiment.[41]

the lattice constant and a transition to a cubic phase from a tetragonal phase, the cubic phase has more compact structure than tetragonal phase. The resistance of the resulting device to humidity was significantly enhanced as the Br content increased, as shown in Fig. 5. When $x = 0.20$ or 0.29, exposure to 55% relative humidity (RH) hardly affected the PCE of the cell. In addition, Br not only broadened the conduction band but also improved the electron extension in the crystal lattice, resulting in increased PCE.[41]

FA and Br intervention forms a perovskite material with a stable structure. Yang et al. and Jeon et al.[43,44] partially used FA instead of MA at A sites and Br instead of I at X sites, thereby improving the stability of the cell while increasing its PCE to over 18%.

3.1.2 *Inorganic perovskites*

Inorganic ions generally have better thermal stability than organic ions, and many researchers have experimented with doping inorganic components at the A site to form stable perovskite compounds. McMeekin et al.[45] partially replaced FA with the inorganic ion Cs and prepared a $FA_{0.83}Cs_{0.17}Pb(I_{1-x}Br_x)_3$ perovskite cell with a band gap of 1.75 eV on the basis of doping with Br. Under standard 1.5 AM sunlight irradiation, the short-circuit current density of the cells reached 19.4 mA/cm^2, and its PCE exceeded 17%. The $FA_{0.83}Cs_{0.17}Pb(I_{0.6}Br_{0.4})_3$ lattice was observed to be most stable under a thermal stress of 130°C. Similarly, Yi et al.[46] designed a $Cs_{0.2}FA_{0.8}PbI_{2.84}Br_{0.16}$ PSC. Figure 6 shows that this cell has excellent air stability in addition to thermal stability.

Nam et al.[47] reported a K-doped all-inorganic Cs-Pb halide perovskite $Cs_{1-x}K_xPbI_2Br$. Doping of K ions not only promotes the formation and transport of photoexcited carriers but also shrinks the PbX_6 octahedron volume. Thus, the phase stability is improved, and the life of the cell in air is prolonged. However, poor coverage and low PCE are among the disadvantages of this technique. Dong et al.[48] proposed an antisolvent-assisted multistep deposition method to prepare high-quality all-inorganic perovskite $CsPbI_2Br$. Figure 7 presents the PbI_2 precursor solution [solvent = dimethyl sulfoxide (DMSO) and dimethylformamide] that is first spin-coated on the substrate. The antisolvent chlorobenzene or ethanol is then added dropwise during spin-coating to form a porous PbI_2 (with DMSO) intermediate phase. The CsBr solution is filled into the pores and fully reacts to deposit a dense, full-coverage $CsPbI_2Br$ film. This method solves the shortcomings of poor shape, low crystallinity, and low coverage of $CsPbI_2Br$ prepared via the traditional one-step spin-coating process and improves the conversion efficiency of the resulting battery to 10.21%. This process also creates a new record for the $CsPbI_2Br$ cells without an HTL. Moreover, the devices displayed good long-term stability in stability tests, no significant efficiency degradation was observed in unpackaged cells after 44 days of exposure to the environment.

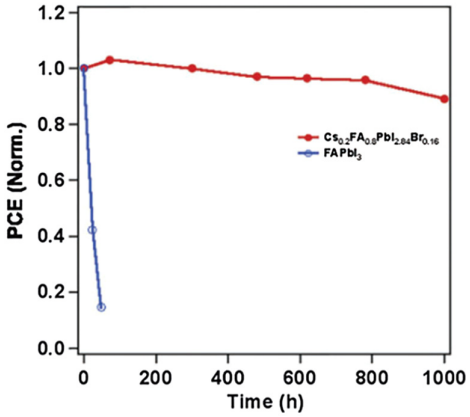

Fig. 6 Comparison of the stability of $Cs_{0.2}FA_{0.8}PbI_{2.84}Br_{0.16}$ and $FAPbI_3$ PSCs. Both devices are not packaged and stored in a dark environment.[46]

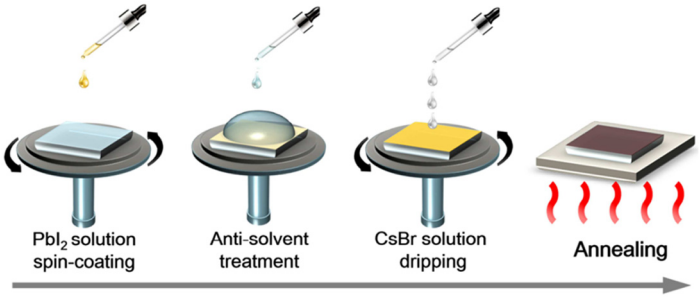

Fig. 7 Schematic of the preparation of $CsPbI_2Br$ by antisolvent-assisted step deposition.[48]

3.1.3 *Pb-free perovskites*

Most mixed perovskite materials contain the toxic heavy metal Pb. If used improperly, Pb could pollute the environment and endanger human health. Therefore, a number of researchers have attempted to replace Pb ions with other inorganic cations and produce environment-friendly Sn-based perovskites. Yang et al.[49] developed a high-performance low-Eg (<1.4 eV) $MA_{0.5}FA_{0.5}Pb_{0.75}Sn_{0.25}I_3$ perovskite cell. The resulting cells were stable in N_2 but not ideal in air because Sn^{2+} in the hybrid Sn-Pb perovskite is easily oxidized to Sn^{4+}. Lee et al.[50] added SnF_2 and pyrazine as inhibitors to Sn-based perovskite to reduce Sn^{4+} formation. This method greatly improved the stability of the Sn-based perovskite cells with high reproducibility. Under ambient condition, the packaged device stored in the dark maintained 98% of its initial conversion efficiency after 100 days.

Gao et al.[51] used a structural adjustment strategy to inhibit the oxidation of Sn^{2+} ions in $FASnI_3$ perovskite cells. Inserting Cs into the $FASnI_3$ crystal structure caused crystal shrinkage, improved crystal symmetry and stability, and reduced the free energy and trap state density of the resulting crystals. More importantly, the fully Pb-free $Cs_xFA_{1-x}SnI_3$ perovskite cells exhibited better long-term stability, including thermal stability, and air stability, in contrast to Cs-free perovskites.

3.2 *Additive Method*

The surface morphology and grain boundary behavior of perovskite crystals can affect their stability and be improved by using additives.

Perovskite materials are particularly sensitive to environmental humidity, and $CH_3NH_3PbI_3$ is hydrophilic, resulting in its easy degradation. Wang et al.[52] passivated $FAPbI_3$ perovskite by adding a phenylalkylamine containing a benzene ring and amino group to the perovskite

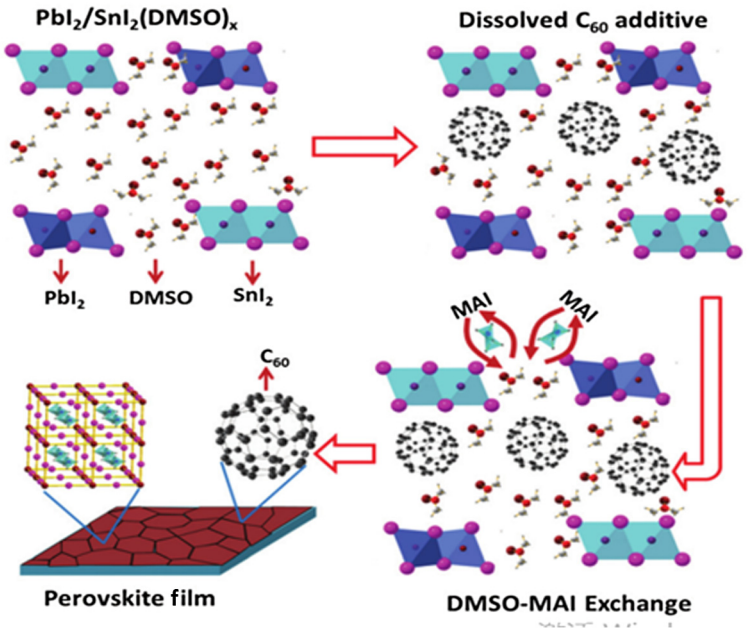

Fig. 8 Schematic representation of C_{60} additive-assisted crystallization of $MAPb_{1-x}Sn_xI_3$ film.[55]

precursor solution. Here, phenylalkylamine was fixed on the PbI_2 substrate by coordination of amino groups with Pb ions and H bonding with I ions because the benzene ring is hydrophobic. Thus, the modified perovskite features moisture resistance. When stored at an ambient condition with $50 \pm 5\%$ RH, the modified $FAPbI_3$ cells showed almost no decrease in PCE after 2800 h. By contrast, the unmodified cells were completely degraded after 90 h under the same conditions. Park et al.[53] used $PC_{61}BM$ as a perovskite additive to passivate the surface defects of $CH_3NH_3PbI_{3-x}Cl_x$ perovskite crystals. $PC_{61}BM$ is located at grain boundaries and found to induce electron-transfer reactions with halogens in the perovskite, tightly bound halogen atoms at the grain boundary to the crystal lattice to prevent them from precipitating from the crystal lattice. The halogens do not leave the crystal lattice but form ion bonding in the perovskite crystal. When these halogens become covalently bonded to a heavy $PC_{61}BM$ molecule, their migration driven by thermal energy is impeded. As a result, the thermal stability of the $CH_3NH_3PbI_{3-x}Cl_x$ perovskite crystal is increased, and less grain boundary is generated, achieving a perovskite grain size of over 150 μm. At the same time, the inverted PSC structure prepared by the method does not require coating with the PCBM ETL, simplifying the preparation.

Liu et al.[54] added C_{60} to a mixed Sn-Pb perovskite film to reduce the number of pores produced during perovskite crystallization. Figure 8 shows the action of C_{60}. The presence of binding energy between C_{60} and DMSO molecules is expected to tune the crystallization process of perovskites, reducing the pores and passivating the interface of the perovskite film. The C_{60} on the grain boundary prevents moisture and oxygen in the surrounding air from penetrating the film, thereby improving the stability of the PSC. Similarly, Lin et al.[55] used poly(diallyldimethylammonium chloride) (PDDA) as a crystal capping agent. PDDA helps control the growth and film formation of perovskites through its cross-linking effect on hydrogen bonds and template effect. This strategy can improve the crystallinity of the resulting film and reduce grain boundary defects and roughness. Improvements in crystal surface morphology and extension of carrier lifetimes are the main reasons behind the improved stability of the final device.

Fairfield et al.[56] added polymers [i.e., polyethylene glycol, polyethyleneimine, poly(acrylic acid), and polyvinylpyrrolidone] to $MAPbI_3$ PSC active layers to increase stability. The polymers tend to suppress the formation of a hydrate crystal phase that accelerates the degradation reaction. The device added with poly(acrylic acid) shows the best stability under humid air and ambient illumination conditions. Perovskite poly(acrylic acid) hybrid solar cells maintained stable efficiency for the first 3 days and then slowly degraded over the next 6 days under humid air and illumination, whereas the control PSCs degraded entirely within the first 2 days.

Yang et al.[57] introduced additional I^- ions to an organic cation precursor solution and formed a perovskite layer through intramolecular exchange. This method greatly reduces the density of defect states and yields ultrahigh-performance PSC devices with better thermal stability and a PCE of 22.1%. Zhang et al.[58] subsequently enhanced the stability of PSCs and achieved a PCE of 21% by inducing the δ-$FAPbI_3$ phase in $MAPbI_3$ films to passivate the trap state and limit ion diffusion in the perovskite phase.

3.3 *Two-Dimensional Perovskites*

Using 2-D perovskite materials in PSCs is considered to be effective for passivating defects and achieving stability. Smith et al.[59] developed a 2-D perovskite $(PEA)_2(MA)_2[Pb_3I_{10}]$ with a PCE of only 4.73% but many unique advantages. The 2-D perovskite, for example, could be prepared in air without annealing and easily produce a flat high-quality film with high moisture resistance. The 2-D perovskite fabrication process also features high operability and controllability. Yao et al.[60] prepared a moisture-resistant 2-D PSC with a two-step spin-coating method using the polymer ammonium PEI·HI as an additive to increase the conversion efficiency to over 15%. Zhang et al.[61] doped Cs^+ into the 2-D perovskite $(BA)_2(MA)_3Pb_4I_{13}$ to obtain a new modified 2-D PSC. The grain size of the modified perovskite was larger, and its trap state density was lower than those of undoped devices. As shown in Fig. 9, the devices doped using 5% Cs^+ exhibited better moisture resistance and thermal stability. Unpackaged cells maintained 89% of their initial PCE after exposure in ambient condition with 30% RH for 1400 h. The cells' tolerance to high humidity also greatly improved (under 65% and 85% RH test conditions), and they sustained thermal stability (under 80°C).

Low perovskite dimensions result in a stable structure but wide band gap. Different dimensions of perovskites exhibit different characteristics. Thus, multidimensional combination perovskites have been designed to form a graded perovskite interface that shows synergistic advantages. Fan et al.[62] lead 2-(1H-pyrazol-1-yl) pyridine (PZPY) into a three-dimensional (3-D) Pb halide perovskite precursor to construct a 1-D–3-D hybrid perovskite. Compared with traditional 3-D perovskites, the one-dimensional (1-D) perovskite displayed a lower packing density and a more flexible structure. The 1-D–3-D perovskite exhibited a long photoluminescence decay life and a low carrier recombination rate. Moreover, the multistructured perovskite possessed thermodynamic self-healing ability, and the flexible 1-D component induced perovskite reconstruction by blocking the ion migration channels of A-site ions. 2-D perovskite materials have good stability in photovoltaic devices, but the barrier to charge transport of the layered structure reduces the optoelectronic performance of these devices. Bai et al.[63] used a 3-D–2-D ($MAPbI_3$-$PEA_2Pb_2I_4$)-mixed perovskite structure to enhance humidity and thermal stability and photoelectric performance. The 3-D–2-D graded surface of the perovskite device formed a barrier at the perovskite/$PC_{61}BM$ interface, which suppressed the I^- ion diffusion from the perovskite layer into the $PC_{61}BM$ layer, and then it reacted with Ag electrode, accounting for its substantially enhanced thermal stability. The 3-D–2-D PSC without encapsulation maintained more than 60% of its original PCE under 20% to 30% RH ambient environment after 30 days. By contrast, the 3-D cells were almost completely degraded under the same conditions. The 3-D–2-D graded surface favorably changed the energy level of perovskite, which helped to reduce the recombination that occurred at the interface, resulting in a promoted ultrahigh Voc of 1.17 V and FF of 0.78 with an overall PCE of 19.89%. Grancini et al.[64] fabricated ultrastable perovskite devices by engineering a 2-D/3-D $[HOOC(CH_2)_4NH_3]_2PbI_4/CH_3NH_3PbI_3$ perovskite junction. At first, the 2-D/3-D perovskite forms an exceptional gradually organized multidimensional interface. Then, they replaced the hole transport material (HTM) with the hydrophobic carbon electrodes to develop HTM-free solar cells. This 2-D/3-D interface combines the high stability of 2-D perovskite with the excellent charge transport properties of the 3-D perovskite, enabling the fabrication of efficient and ultrastable solar cells. The fabricated 100-cm^2 solar cells achieved an efficiency of 11.2%, which could last 12,000 h with zero loss under AM 1.5 G illumination at 55°C. Chen et al.[65] designed 2-D–3-D perovskites by *in situ* growth of a $PEA_2Pb_2I_4$ coating on 3-D perovskite films with a higher PCE of 18.51%. This 2-D to 3-D-stacked layered structure helped optimize the band structure and reduced nonradiative recombination in the subgap state. Benefiting from the high moisture resistivity and suppressed

ion migration of the 2-D perovskite, the device also exhibited significantly improved long-term stability, retaining nearly 90% of the initial PCE after 1000 h exposure under ambient conditions with a high RH level of 60%.

The photoelectric performance of 3-D all-inorganic perovskite cells is poor despite their good stability, extensive carrier recombination caused by interfacial defects between the perovskite and HTL is among the reasons cited for this observation.[47,48] Zhang et al.[66] reported the 3-D–2-D–0-D (quantum dot) interfacial structure of the all-inorganic perovskite $CsPbBrI_2$. This grading combination not only improved hole extraction and conduction efficiency but also reduced recombination losses. The conversion efficiency of the device reached 12.39%, which has never before been achieved in all-inorganic $CsPbBrI_2$ PSCs.

4 Hole Transport Layer

The HTL can transport holes and prevent reverse transport of electrons and has a large effect on the efficiency and stability of PSC devices. An ideal HTL has the following characteristics: (1) suitable energy band, (2) high conductivity, (3) full coverage of the perovskite layer, (4) ability to prevent reverse electron transport, (5) good stability, and (6) simple preparation.

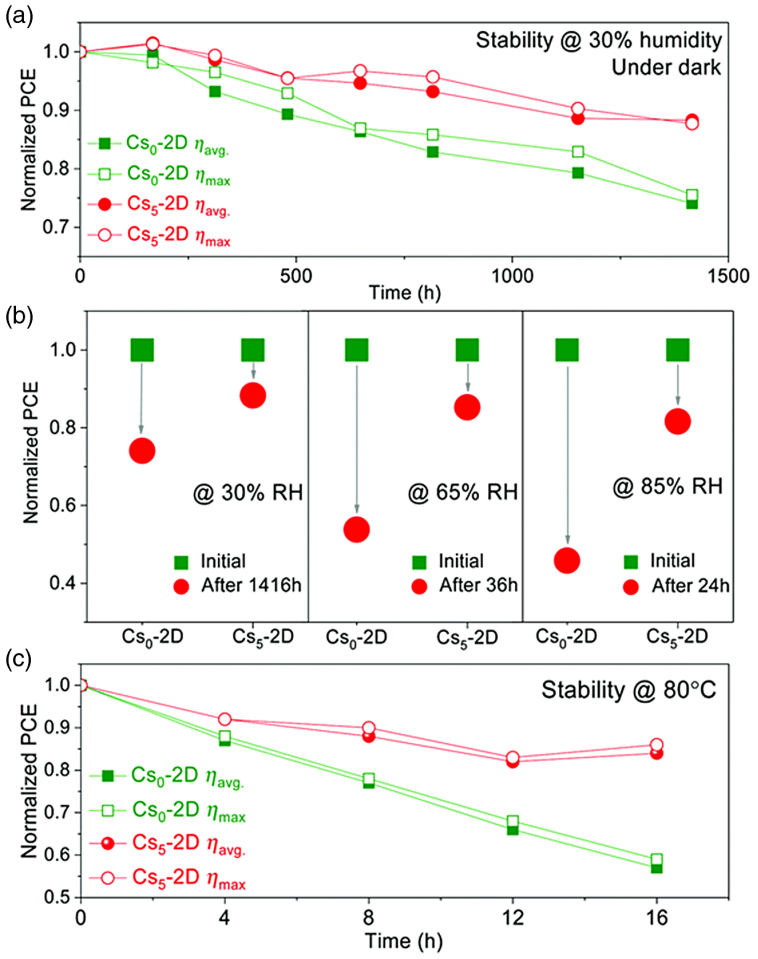

Fig. 9 Stability measurements for the Cs0-2D and Cs5-2D PSCs. (a) Long-term stability measurements of both solar cells without any encapsulation under ambient conditions where the RH is 30% RH. Both the highest performing device and eight average level devices showing slower degradation for the Cs5-2D than the Cs0-2D solar cell as a function of time. (b) Humidity tolerance measurements for both solar cells at different humidities: 30%, 65% and 85% RH. (c) Thermal stability at 80°C under an inert atmosphere without encapsulation for both Cs0-2D and Cs5-2D PSCs.[61]

Kim et al.[67] introduced the solid-state HTM 2,2′,7,7′-tetrakis(N,N′-di-*p*-methoxyphenylamine)-9,9′-spirobifluorene (spiro-OMeTAD) to PSCs for the first time and realized the preparation of all-solid PSCs. To date, spiro-OMeTAD has become the most widely used HTM for perovskite cells. However, similar to the dense layer of TiO_2, spiro-OMeTAD does not protect cells against moisture and oxygen very well, which is not conducive to the long-term stability of these cells. Therefore, strategies to improve the HTL have also been developed.

4.1 *Doping Method*

Doping with suitable additives could improve the performance of devices based on spiro-OMeTAD. Huang et al.[68] doped tetrafluoro-tetracyanoquinodimet-hane (F4-TCNQ) into spiro-MeOTAD by solvent treatment to prepare planar heterojunction PSCs. F4-TCNQ doping improved the conductivity of spiro-MeOTAD and improved the compatibility between the highest occupied molecular (HOMO) level of the transport layer and that of the perovskite layer. F4-TCNQ is hydrophobic and can improve the humidity stability of PSCs. Li et al.[69] studied Cu salt (CuSCN or CuI)-doped spiro-OMeTAD and found that these salts could prevent moisture penetration and improve the stability of PSCs. Wang et al.[70] used CuI as an oxidant for spiro-MeOTAD. CuI has high hole mobility and is inexpensive. Moreover, oxidation of CuI prolongs the effective cell life.

Ma et al.[71] used a Co(III) complex as a dopant that is mainly distributed at the interface between HTL and perovskite to enhance carrier collection and transfer and effectively increase the solar cell efficiency to 17.34%. The cocomplex also suppresses defects, such that there is less degradation of the device with the cocomplex dopant, providing the cell with good thermal stability. The PCE of the doped cells were maintained at 80% or more of the initial value after storage for 9 h at 60°C under 1.5 AM sunlight irradiation in N_2 environment. By contrast, the PCE of the undoped cells decreased to 30% or less of its initial value under the same condition.

Seo et al.[72] used Cu phthalocyanine (CuPc) as a dopant for spiro-MeOTAD because it exhibits good chemical and thermal stability and can effectively prevent reverse electron transport and prolong the carrier lifetime. The use of CuPc yielded a high PCE of 19.4% under exposure to standard 1.5 AM sunlight and certain improvements in the stability of PSCs.

4.2 *Substitution Method*

4.2.1 *Undoped organic HTMs*

When the HTL is prepared by using spiro-MeOTAD, the HTL is usually doped with *p*-type dopants, such as Li-TFSI or tributyl phosphate. Spiro-MeOTAD has poor conductivity and must be doped to increase its conductivity. However, the use of dopants requires complex preparation conditions and increases the preparation cost. Moreover, the dopant is easily deliquescent, which could exert a negative effect on the stability of the HTL and perovskite layer. Thus, developing a high-performance nondoped HTM is a viable method to improve the durability of PSC devices.

Liu et al.[73] used the undoped organic small-molecule tetrathiafulvalene derivative (TTF-1) as an HTM to reduce the cost of fabricating PSCs and obtained a PCE OF 11.03%. This value is equivalent to that of a *p*-type doped spiro-OMeTAD cell. However, the cells based on dopant-free TTF-1 are more stable than the cells based on common *p*-type doping spiro-OMeTAD. The hydrophobic alkyl chains of TTF-1 can increase the resistance of the HTL to humidity, and avoiding the use of deliquescent additives also improves the stability. Figure 10 shows the degradation time associated with a 20% decrease in efficiency, the lifespan of the cells without encapsulation based on dopant-free TTF-1 (∼360 h) was three times higher than that of cells based on *p*-type doping spiro-OMeTAD (∼120 h) under ambient conditions at 40% RH. Liao et al.[74] reported undoped 4,8-dithien-2-yl-benzo[1,2-d;4,5-d′]bistriazole-alt-benzo[1,2-b:4,5-b′]dithiophenes (pBBTa-BDTs) as a polymer HTM. pBBTa-BDT is π-downward oriented on perovskites and arranged in a highly ordered manner. The smooth and dense surface of this HTM can effectively prevent atmospheric moisture from affecting the perovskite layer and inhibit perovskite degradation while effectively extracting and collecting holes.

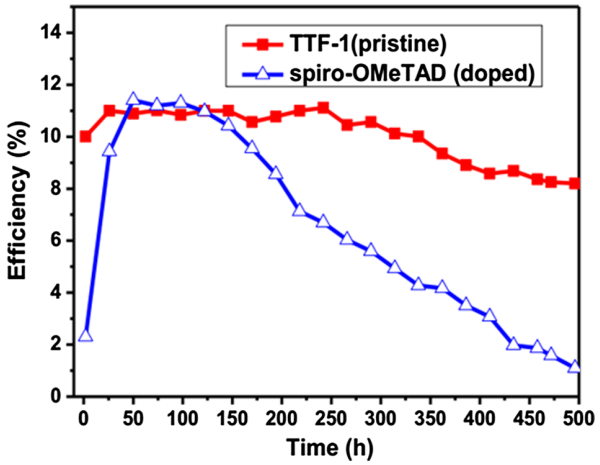

Fig. 10 Efficiency variation of optimized cells based on dopant-free TTF-1 (pristine) and p-type doping spiro-OMeTAD (doped). Unencapsulated cells were stored in air at room temperature with a humidity of about 40% and were measured under illumination at AM 1.5 G.[73]

As an important hole-transporting material, metal phthalocyanines (MPcs) have been widely used in organic solar cells. However, most of these materials are highly insoluble and require preparation via a rigorous thermal evaporation procedure, which may destroy the underlying perovskite layer. Wu et al.[75] synthesized a soluble *tert*-butyl-substituted zinc phthalocyanine ($ZnPc(tBu)_4$) and applied it as an undoped HTL to $MAPbI_3$ PSCs. $ZnPc(tBu)_4$ has high hole mobility and matching HOMO and LUMO energy levels and is tolerant to humidity. It can be spin-coated under ambient conditions (humidity: 30% to 70%). The unpackaged device fabricated from this material retained 85% of its initial PCE after 120 h in the dark at a humidity of 70% to 80%. The disadvantage of this material, however, is that its conversion efficiency is low (approximately only 8%) because $ZnPc(tBu)_4$ has poor coverage and a large number of interfacial defects.

Caliò et al.[76] reported the synthesis of a Cu(II)-based phthalocyanine [$(^tOctPhO)_8CuPc$ 1] with 4-tert-octylphenoxy-substituted functional groups that possesses excellent solubility in a wide range of organic solvents. The $(^tOctPhO)_8CuPc$ 1 and its analogous Zn(II) phthalocyanine [represented as $(^tOctPhO)_8ZnPc$ 2] were applied as HTL in $(FAPbBr_3)_{0.85}(MAPbI_3)_{0.15}$ PSCs. The MPcs exhibit high thermal and chemical stability, which can help to improve the preservation of the underlying perovskite layer. The stability of unencapsulated devices with the configurations of Cu(II) and Zn(II) Pc-based and Spiro-OMeTAD-based PSCs was examined for over 200 h under ambient environment at 25°C and an RH of 50% to 60%. The PCE of PSCs with $(^tOctPhO)_8CuPc$ 1 as the HTM only lost less than 10% of the initial value after 7 days. The $(^tOctPhO)_8ZnPc$ 2-based devices dropped 15% of their initial value, whereas the reference devices with Spiro-OMeTAD lost over 20% of their initial efficiency value.

Liu et al.[77] used CuPc as an HTM in $CsPbBr_3$ perovskite cells, increasing their efficiency by 60%. $CsPbBr_3$ itself is an all-inorganic perovskite with good thermal stability and durability. The high coverage of CuPc can also exert hydrophobic effects. The overall device can exhibit excellent stability at high humidity and temperature. A schematic of the cell structure and normalized PCE over time is shown in Fig. 11. Feng et al.[78] have recently used high-solubility arylamine groups [triphenylamine (TPA) and diphenylamine (DPA)] as substituents. They designed two dopant-free HTMs based on CuPc derivatives: the methoxydiphenylamine-substituted copper phthalocyanine (OMe-DPA-CuPc) and the methoxytriphenylamine-substituted copper phthalocyanine (OMe-TPA-CuPc). The HTM/perovskite interaction occurs at the methoxy (OMe) group interface with the perovskite methylammonium sites, which improves the performance of PSCs due to the strong adhesion and enhanced interfacial coupling between HTMs and perovskites. Researchers used $Cs_{0.05}(MA_{0.13}FA_{0.87})_{0.95}Pb(I_{0.87}Br_{0.13})_3$ as absorption layer and OMe-TPA-CuPc as undoped HTM layer, achieving a PCE of 19.7% for the fabricated PSCs under 1 sun illumination. Devices based on OMe-DPA-CuPc HTM showed lower PCEs (16.7%) than PSCs using OMe-TPA-CuPc HTM. The fabricated PSCs based on substituted

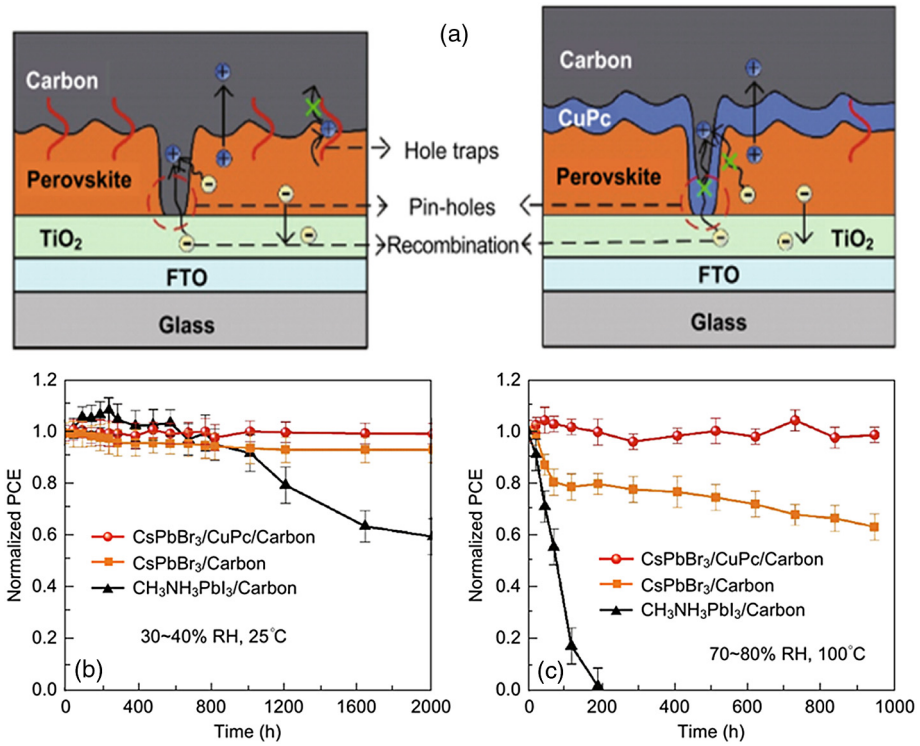

Fig. 11 Use of CuPc as an HTL in CsPbBr3 cells. (a) Functional diagram of CuPc. (b) Normalized images of the PCEs of PSCs based on $CsPbBr_3$/CuPc/carbon, $CsPbBr_3$/carbon, and $CH_3NH_3PbI_3$/carbon versus storage time in ambient air (30% to 40% RH, 25°C) without encapsulation. (c) Normalized images of the PCEs of PSCs based on $CsPbBr_3$/CuPc/carbon, $CsPbBr_3$/carbon, and $CH_3NH_3PbI_3$/carbon versus storage time heated at high temperature (100°C) in a high-humidity ambient environment (70% to 80% RH, 100°C) without encapsulation.[77]

CuPc exhibited considerably better stabilities than the doped Spiro-OMeTAD-based ones. When exposed to atmosphere with a humidity of 75% and at room temperature for more than 960 h, the devices based on OMe-DPA-CuPc HTM or OMe-TPA-CuPc HTM only dropped to 92% and 89% of their initial PCEs, respectively. By contrast, the PCE of doped Spiro-OMeTAD-based PSCs dropped to 50% of the initial value after 480 h.

4.2.2 *Inorganic HTMs*

Some organic HTMs require complex synthesis processes, are sensitive to the environment, and have poor chemical stability. The use of a stable inorganic HTM, i.e., a metal oxide *p*-type HTM, such as NiO_x and CrO_x. Islam et al.[79] found that NiO_x exhibits better properties than commonly used PEDOT:PSS as an HTM in inverted-structured PSCs. PEDOT:PSS is acidic and hygroscopic, easily leading to perovskite degradation. NiO_x itself has outstanding thermal and chemical stability with a large band gap and good transmittance. Researchers had sputtered a 70-nm-thick NiO_x film onto ITO glass and found that the NiO_x conductivity is higher when the Ni^{3+}/Ni^{2+} ratio is high. However, the optical transmittance of the material was reduced at the same time. The PCE of PSCs prepared after optimization reached 15.2%. The encapsulated cells using NiO_x as an HTM could maintain more than 73% of the initial PCE at 30°C and under 50% RH for more than 1000 h. In addition, the packaged device did not degrade after 1000 h of storage in the dark at 85°C (~5% RH). Degradation under illumination occurs because NiO_x is unstable under UV light. Qin et al.[80] introduced CrO_x to a planar inverted-structure PSC as an HTL. Similar to NiO_x, CrO_x exhibits better stability than PEDOT:PSS, and the stability of final device with CrO_x HTM was also better. Cu was used as a dopant for CrO_x, Cu could increase the conductivity of CrO_x and inhibit its reaction with the degraded perovskite product. Compared CrO_x with NiO_x, the PCE of the Cu-doped CrO_x device is ~11% while that of the Cu-doped NiO_x device is 15.4%.[81]

Besides thermal and humidity stability, light stability is another direction of cell stability. To prevent the decomposition of perovskite materials caused by UV light, Zhang et al.[82] proposed the use of $CuCrO_2$ as an HTL. $CuCrO_2$ is capable of achieving broad absorption in the UV region and high transmittance at wavelengths above 400 nm, thereby preventing the perovskite layer from being decomposed by UV light without affecting its light absorption properties.

4.2.3 *Graphene oxide*

Yeo et al.[83] developed a reduced graphene oxide (RGO) film as an HTL. RGO exhibits high conductivity and can promote charge collection and delay recombination. Given that RGO is nearly neutral with few surface oxygen functional groups, it is stable in nature, does not degrade perovskite similar to acidic PEDOT:PSS, and does not promote decomposition under UV light like NiO_x. Whereas NiO_x requires high-temperature and high-vacuum conditions to prepare, RGO can be prepared by the solution method at low cost. More importantly, the passivation effect of RGO can effectively reduce the decomposition of $CH_3NH_3PbI_3$ perovskite films caused by oxygen and water, enhance their stability, and prolong cell life. GO has a high oxygen content, which results in low electrical conductivity and is disadvantageous for HTMs. To reduce the oxygen content of this material, Yang et al.[84] reported a method to balance the functionality and conductivity of GO films by limiting its thickness. The thinner GO film resulted in higher conductivity, and the group grew a large-sized perovskite crystal of 500 to 1000 nm on the 2-nm GO film. Larger grains can effectively suppress the charge recombination due to the reduced concentration of grain boundaries. This method achieved a PCE of 16.5% without hysteresis. In addition, the encapsulated GO perovskite cells stored in the dark could maintain over 80% of its initial PCE value after 2000 h under ambient conditions at 80% RH. By contrast, the PCE of PEDOT:PSS-based device rapidly decreased to 40% of the initial PCE after just 1400 h under the same condition.

4.3 *Composite Structure Method*

Spiro-OMeTAD is generally hydrophilic and does not prevent moisture from entering the perovskite layer. The most commonly used HTM in inverted-structured cells is PEDOT:PSS. However, PEDOT:PSS not only absorbs water but is also acidic in aqueous solution and could easily erode the ITO electrode. Therefore, composite HTLs have been prepared by combining the different properties of two materials to enhance the HTL or overall stability.

Hou et al.[85] used a MoO_3/PEDOT:PSS double-layered structure to enhance the stability of PSCs. Here, the MoO_3 layer is applied between ITO and PEDOT:PSS. MoO_3 is nontoxic and stable under environmental conditions; it can completely eliminate direct contact between the ITO and PEDOT:PSS and protect the ITO electrode while improving hole extraction efficiency. Lee et al.[86] designed a GO/PEDOT:PSS double-layer HTL. GO possesses excellent stability but, when applied to the HTL alone, results in an uneven coating on the ITO that could deteriorate the morphology of perovskite with holes and leakage. The double-layered structure avoids this defect while isolating ITO and PEDOT:PSS. In addition, CuPc/PEDOT:PSS composite HTLs[87] and CuI/PEDOT:PSS double layer HTLs[88] with an inverted structure have also been proposed. The performance of cells fabricated with these layers is improved compared with that of a single-layer HTL. The complementary effect between CuI and PEDOT:PSS is especially obvious. CuI provides good hydrophobicity and environmental stability and isolates the ITO and PEDOT:PSS. PEDOT:PSS passivates the defect state in the interface between the CuI and perovskite layers. In initial tests, the device efficiency increased from 12.9% for a single PEDOT:PSS to 14.4% for the double-layered structure. The CuI-PEDOT HTL-based devices showed better stability than the PEDOT:PSS-based devices. After 720 h of storage in a glovebox, the PCE of PEDOT:PSS-based devices without encapsulation decreased by 28% of the initial efficiency, whereas the PCE of CuI-PEDOT HTL-based devices only decreased by 12%.

Compared with GO, RGO has better energy level matching and higher conductivity. Luo et al.[89] applied an RGO/nondoped spiro-OMeTAD double-layer structured HTL to a PSC. The RGO was used to block moisture and oxygen and improve the hole transport and collection efficiency of the HTL. After 500 h of storage under ambient environment at 20°C, 40% RH, the

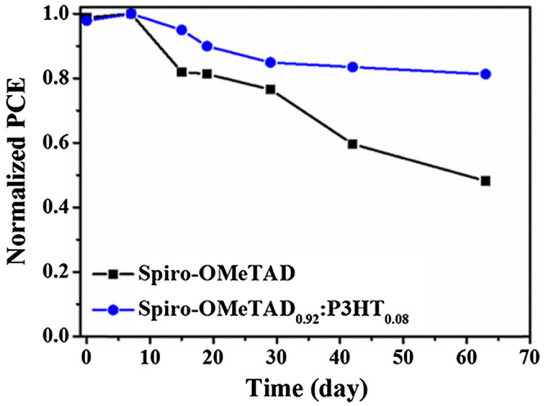

Fig. 12 Stability test of each HTL device at 30% RH.[90]

PCE of the resulting cells decreased by only 15% of their initial value. Kim et al.[90] designed a graded hybrid HTL with a spiro-OMeTAD and P3HT blend spin-coated on the perovskite layer. The mixed HTL displayed good vertical stratification, and the hydrophilic spiro-OMeTAD was distributed in the lower layer close to the perovskite surface. The hydrophobic P3HT was also distributed in the upper layer in contact with air, thereby preventing moisture penetration and improving the stability of the final cells. The moisture stability of unencapsulated PSCs was tested at ~30% RH (Fig. 12), the efficiency of the mixed HTM device decreases more slowly than that of the spiro-OMeTAD device.

5 Summary and Outlook

The depletion of fossil fuels provides an excellent opportunity to develop photovoltaic cells. PSCs are among the most promising candidates for next-generation energy sources. After years of development, researchers of PSCs have made considerable breakthroughs. This paper summarizes studies aiming to improve the stability of perovskite cells. Especially for the humidity stability and thermal stability, some of the developed methods include: (1) changing the physicochemical properties of perovskites by doping or ion addition and then improving the stability of the perovskite layer; (2) using an alternative strategy to switch to a stable inorganic perovskite; (3) modifying the ETL or HTL, or using more stable materials as ETM or HTM; and (4) designing a multilayer structure to isolate the external environment and protect the perovskite layer.

These works have studied the methods to improve the stability of PSCs from various aspects and have reference value for the future research. Among them, we believe that the following directions have high research value. First, ZnO has good photoelectric properties as ETM, and its environmental stability is good. But it will react with the perovskite and generate more defects at the interface. We can modify ZnO to passivate the defect or find a suitable intermediate layer to avoid direct contact between ZnO and perovskites. Second, some of the inorganic perovskites appear to have good thermal stability. It is expected to develop a stable and efficient inorganic perovskite cell if we solve some defects of inorganic perovskite, such as phase instability for $CsPbI_3$ and high bandgaps for $CsPbBr_3$. For example, we can research for new inorganic components with appropriate antisolvent formulations. Third, development of low-dimensional perovskite, including 2-D perovskite and quantum dot perovskite; low-dimensional perovskites have stable structure and high film quality with high repeatability, which facilitates the large-scale production of future perovskite cells. One of the most important challenges of low-dimensional perovskite is solving the charge carriers transport issues. Last but not the least, RGO is stable, conductive, and easy to prepare. In addition to its use as an HTM, we can apply it in other parts of the cell, such as ETL or intermediate layers, using RGO to strengthen the stability.

To realize the commercialization of PSCs, improving the long-term stability of these cells is an important challenge. Material, structural, and fabrication innovations must be combined to continuously explore new strategies to stabilize PSCs and provide a new renewable energy technology.

References

1. A. Kojima et al., "Organometal halide perovskites as visible-light sensitizers for photovoltaic cells," *J. Am. Chem. Soc.* **131**, 6050–6051 (2009).
2. NREL, "Best research-cell efficiency chart," 2019, https://www.nrel.gov/pv/cell-efficiency.html.
3. G. Divitini et al., "*In situ* observation of heat-induced degradation of perovskite solar cells," *Nat. Energy* **1**, 15012 (2016).
4. A. Alberti et al., "Revealing a discontinuity in the degradation behaviour of $CH_3NH_3PbI_3$ during thermal operation," *J. Phys. Chem. C* **121**, 13577–13585 (2017).
5. S. Bae et al., "Electric-field-induced degradation of methylammonium lead iodide perovskite solar cells," *J. Phys. Chem. Lett.* **7**(16), 3091–3096 (2016).
6. L. Meng et al., "Recent advances in the inverted planar structure of perovskite solar cells," *Acc. Chem. Res.* **49**(1), 155–165 (2016).
7. H. J. Jung et al., "Self-passivation of 2-D Ruddlesden–Popper perovskite by polytypic surface PbI_2 encapsulation," *Nano Lett.* **19**, 6109–6117 (2019).
8. R. Fan et al., "Novel flexible photoanode based on Ag nanowire/polymer composite electrode," *J. Mater. Sci. Mater. Electron.* **28**(14), 10092–10097 (2017).
9. S. K. Pathak et al., "Performance and stability enhancement of dye-sensitized and perovskite solar cells by Al doping of TiO_2," *Adv. Funct. Mater.* **24**(38), 6046–6055 (2014).
10. G. Yin et al., "Enhancing efficiency and stability of perovskite solar cells through Nb-doping of TiO_2 at low temperature," *ACS Appl. Mater. Interfaces* **9**(12), 10752–10758 (2017).
11. J. Peng et al., "Efficient indium-doped TiO_x electron transport layers for high-performance perovskite solar cells and perovskite-silicon tandems," *Adv. Energy Mater.* **7**(4), 1601768 (2017).
12. J. Y. Jeng et al., "$CH_3NH_3PbI_3$ perovskite/fullerene planar-heterojunction hybrid solar cells," *Adv. Mater.* **25**(27), 3727–3732 (2013).
13. J. You et al., "Low-temperature solution-processed perovskite solar cells with high efficiency and flexibility," *ACS Nano* **8**(2), 1674–1680 (2014).
14. P. Docampo et al., "Efficient organometal trihalide perovskite planar-heterojunction solar cells on flexible polymer substrates," *Nat. Commun.* **4**, 2761 (2013).
15. J. H. Heo et al., "Hysteresis-less inverted $CH_3NH_3PbI_3$ planar perovskite hybrid solar cells with 18.1% power conversion efficiency," *Energy Environ. Sci.* **8**(5), 1602–1608 (2015).
16. C.-Z. Li et al., "Modulate hybrid organic–perovskite photovoltaic performance by controlling the excited dynamics of fullerenes," *Mater. Horizons* **2**(4), 414–419 (2015).
17. Y. Bai et al., "Enhancing stability and efficiency of perovskite solar cells with crosslinkable silane-functionalized and doped fullerene," *Nat. Commun.* **7**, 12806 (2016).
18. K. O. Brinkmann et al., "Suppressed decomposition of organometal halide perovskites by impermeable electron-extraction layers in inverted solar cells," *Nat. Commun.* **8**, 13938 (2017).
19. D. Y. Liu and T. L. Kelly, "Perovskite solar cells with a planar heterojunction structure prepared using room-temperature solution processing techniques," *Nat. Photonics* **8**(2), 133–138 (2014).
20. D. Yang et al., "High efficiency planar-type perovskite solar cells with negligible hysteresis using EDTA-complexed SnO_2," *Nat. Commun.* **9**(1), 3239 (2018).
21. I. Hwang and K. Yong, "Novel CdS hole-blocking layer for photostable perovskite solar cells," *ACS Appl. Mater. Interfaces* **8**(6), 4226–4232 (2016).
22. W. Qiu et al., "High efficiency perovskite solar cells using a PCBM/ZnO double electron transport layer and a short air-aging step," *Organic Electron.* **26**, 30–35 (2015).
23. E. Singh and H. S. Nalwa, "Graphene-based bulk-heterojunction solar cells: a review," *J. Nanosci. Nanotechnol.* **15**(9), 6237–6278 (2015).
24. E. Singh and H. S. Nalwa, "Stability of graphene-based heterojunction solar cells," *RSC Adv.* **5**(90), 73575–73600 (2015).
25. E. Singh and H. S. Nalwa, "Graphene-based dye-sensitized solar cells: a review," *Sci. Adv. Mater.* **7**(10), 1863–1912 (2015).

26. A. Agresti et al., "Efficiency and stability enhancement in perovskite solar cells by inserting lithium-neutralized graphene oxide as electron transporting layer," *Adv. Funct. Mater.* **26**(16), 2686–2694 (2016).
27. S. Song et al., "Systematically optimized bilayered electron transport layer for highly efficient planar perovskite solar cells ($\eta = 21.1\%$)," *ACS Energy Lett.* **2**(12), 2667–2673 (2017).
28. I. Hwang, M. Baek, and K. Yong, "Core/shell structured TiO2/CdS electrode to enhance the light stability of perovskite solar cells," *ACS Appl. Mater. Interfaces* **7**(50), 27863–27870 (2015).
29. J. A. Christians, P. A. M. Herrera, and P. V. Kamat, "Transformation of the excited state and photovoltaic efficiency of $CH_3NH_3PbI_3$ perovskite upon controlled exposure to humidified air," *J. Am. Chem. Soc.* **137**(4), 1530–1538 (2015).
30. Z. Song et al., "Perovskite solar cell stability in humid air: partially reversible phase transitions in the PbI_2-CH_3NH_3I-H_2O system," *Adv. Energy Mater.* **6**(19), 1600846 (2016).
31. Z. Ahmad et al., "Degradation analysis in mixed ($MAPbI_3$ and $MAPbBr_3$) perovskite solar cells under thermal stress," *J. Mater. Sci. Mater. Electron.* **30**, 1354–1359 (2019).
32. Y. Zhou et al., "Thermal stress analysis of mesoporous perovskite solar cell by finite element method," in *16th Int. Conf. Electron. Packaging Technol.*, IEEE (2015).
33. D. Bryant et al., "Light and oxygen induced degradation limits the operational stability of methylammonium lead triiodide perovskite solar cells," *Energy Environ. Sci.* **9**(5), 1655–1660 (2016).
34. N. Aristidou et al., "Fast oxygen diffusion and iodide defects mediate oxygen-induced degradation of perovskite solar cells," *Nat. Commun.* **8**, 15218 (2017).
35. G. Mannino et al., "First evidence of $CH_3NH_3PbI_3$ optical constant improvement in N_2 environment in the range 40–80°C," *J. Phys. Chem. C* **121**(14), 7703–7710 (2017).
36. S. Y. Luchkin et al., "Reversible and irreversible electric field induced morphological and interfacial transformations of hybrid lead iodide perovskites," *ACS Appl. Mater. Interfaces* **9**(39), 33478–33483 (2017).
37. M. V. Khenkin et al., "Bias-dependent degradation of various solar cells: lessons for stability of perovskite photovoltaics," *Energy Environ. Sci.* **12**(2), 550–558 (2019).
38. F. Li et al., "Machine learning (ML)-assisted design and fabrication for solar cells," *Energy Environ. Mater.* 1–12 (2019).
39. M. V. Khenkin et al., "Reconsidering figures of merit for performance and stability of perovskite photovoltaics," *Energy Environ. Sci.* **11**(4), 739–743 (2018).
40. A. Mei et al., "A hole-conductor-free, fully printable mesoscopic perovskite solar cell with high stability," *Sci. Found. China* **345**(6194), 295–298 (2014).
41. E. M. Talbert et al., "Bromine substitution improves excited-state dynamics in mesoporous mixed halide perovskite films," *Nanoscale* **9**(33), 12005–12013 (2017).
42. J. H. Noh et al., "Chemical management for colorful, efficient, and stable inorganic-organic hybrid nanostructured solar cells," *Nano Lett.* **13**(4), 1764–1769 (2013).
43. W. S. Yang et al., "SOLAR CELLS. High-performance photovoltaic perovskite layers fabricated through intramolecular exchange," *Science* **348**, 1234–1237 (2015).
44. N. J. Jeon et al., "Compositional engineering of perovskite materials for high-performance solar cells," *Nature* **517**, 476–480 (2015).
45. D. McMeekin et al., "A mixed-cation lead mixed-halide perovskite absorber for tandem solar cells," *Science* **351**, 151–155 (2016).
46. C. Yi et al., "Entropic stabilization of mixed a-Cation ABX_3 metal halide perovskites for high performance perovskite solar cells," *Energy Environ. Sci.* **9**(2), 656–662 (2016).
47. J. K. Nam et al., "Potassium incorporation for enhanced performance and stability of fully inorganic cesium lead halide perovskite solar cells," *Nano Lett.* **17**(3), 2028–2033 (2017).
48. C. Dong et al., "Anti-solvent assisted multi-step deposition for efficient and stable carbon-based $CsPbI_2Br$ all-inorganic perovskite solar cell," *Nano Energy* **59**, 553–559 (2019).
49. Z. Yang et al., "Stable low-bandgap Pb-Sn binary perovskites for tandem solar cells," *Adv. Mater.* **28**(40), 8990–8997 (2016).
50. S. J. Lee et al., "Fabrication of efficient formamidinium tin iodide perovskite solar cells through SnF_2-pyrazine complex," *J. Am. Chem. Soc.* **138**(12), 3974–3977 (2016).

51. W. Gao et al., "Robust stability of efficient lead-free formamidinium tin iodide perovskite solar cells realized by structural regulation," *J. Phys. Chem. Lett.* **9**(24), 6999–7006 (2018).
52. F. Wang et al., "Phenylalkylamine passivation of organolead halide perovskites enabling high-efficiency and air-stable photovoltaic cells," *Adv. Mater.* **28**, 9986–9992 (2016).
53. C. Park et al., "Organometal halide perovskite solar cells with improved thermal stability via grain boundary passivation using a molecular additive," *Adv. Funct. Mater.* **27**, 1703546 (2017).
54. C. Liu et al., "C_{60} additive-assisted crystallization in $CH_3NH_3Pb_{0.75}Sn_{0.25}I_3$ perovskite solar cells with high stability and efficiency," *Nanoscale* **9**(37), 13967–13975 (2017).
55. Z. Lin et al., "Enhanced planar heterojunction perovskite solar cell performance and stability using PDDA polyelectrolyte capping agent," *Sol. Energy Mater. Sol. Cells* **172**, 133–139 (2017).
56. D. J. Fairfield et al., "Structure and chemical stability in perovskite–polymer hybrid photovoltaic materials," *J. Mater. Chem. A* **7**(4), 1687–1699 (2019).
57. W. S. Yang et al., "Iodide management in formamidinium-lead-halide-based perovskite layers for efficient solar cells," *Science* **356**(6345), 1376–1379 (2017).
58. Y. Zhang et al., "Trash into treasure: δ-$FAPbI_3$ polymorph stabilized $MAPbI_3$ perovskite with power conversion efficiency beyond 21%," *Adv. Mater.* **30**, 1707143 (2018).
59. I. C. Smith et al., "A layered hybrid perovskite solar-cell absorber with enhanced moisture stability," *Angew. Chem. Int. Ed.* **53**(42), 11232–11235 (2014).
60. K. Yao et al., "Mixed perovskite based on methyl-ammonium and polymeric-ammonium for stable and reproducible solar cells," *Chem. Commun.* **51**(84), 15430–15433 (2015).
61. X. Zhang et al., "Stable high efficiency two-dimensional perovskite solar cells via cesium doping," *Energy Environ. Sci.* **10**(10), 2095–2102 (2017).
62. J. Fan et al., "Thermodynamically self-healing 1D-3D hybrid perovskite solar cells," *Adv. Energy Mater.* **8**(16), 1703421 (2018).
63. Y. Bai et al., "Dimensional engineering of a graded 3D-2D halide perovskite interface enables ultrahigh V_{oc} enhanced stability in the p-i-n photovoltaics," *Adv. Energy Mater.* **7**(20), 1701038 (2017).
64. G. Grancini et al., "One-year stable perovskite solar cells by 2D/3D interface engineering," *Nat. Commun.* **8**, 15684 (2017).
65. P. Chen et al., "*In situ* growth of 2D perovskite capping layer for stable and efficient perovskite solar cells," *Adv. Funct. Mater.* **28**, 1706923 (2018).
66. J. Zhang et al., "3D-2D-0D interface profiling for record efficiency all-inorganic $CsPbBrI_2$ perovskite solar cells with superior stability," *Adv. Energy Mater.* **8**(15), 1703246 (2018).
67. H. S. Kim et al., "Lead iodide perovskite sensitized all-solid-state submicron thin film mesoscopic solar cell with efficiency exceeding 9%," *Sci. Rep.* **2**, 591 (2012).
68. L. Huang et al., "Efficient and stable planar perovskite solar cells with a non-hygroscopic small molecule oxidant doped hole transport layer," *Electrochim. Acta* **196**, 328–336 (2016).
69. M. Li et al., "Copper salts doped spiro-OMeTAD for high-performance perovskite solar cells," *Adv. Energy Mater.* **6**(21), 1601156 (2016).
70. P. Wang et al., "Copper iodide as a potential low-cost dopant for spiro-MeOTAD in perovskite solar cells," *J. Mater. Chem. C* **4**(38), 9003–9008 (2016).
71. Y. Ma et al., "Enhanced charge collection and stability in planar perovskite solar cells based on a cobalt(iii)-complex additive," *RSC Adv.* **7**(60), 37654–37658 (2017).
72. J. Seo et al., "Effective electron blocking of CuPC-doped spiro-OMeTAD for highly efficient inorganic-organic hybrid perovskite solar cells," *Adv. Energy Mater.* **5**, 1501320 (2015).
73. J. Liu et al., "A dopant-free hole-transporting material for efficient and stable perovskite solar cells," *Energy Environ. Sci* **7**(9), 2963–2967 (2014).
74. H.-C. Liao et al., "Dopant-free hole transporting polymers for high efficiency, environmentally stable perovskite solar cells," *Adv. Energy Mater.* **6**, 1600502 (2016).
75. S. Wu et al., "Low cost and solution-processable zinc phthalocyanine as alternative hole transport material for perovskite solar cells," *RSC Adv.* **6**(109), 107723–107731 (2016).

76. L. Caliò et al., "Cu(ii) and Zn(ii) based phthalocyanines as hole selective layers for perovskite solar cells," *Sustainable Energy Fuels* **1**(10), 2071–2077 (2017).
77. Z. Liu et al., "Efficient carbon-based $CsPbBr_3$ inorganic perovskite solar cells by using Cu-phthalocyanine as hole transport material," *Nano-Micro Lett.* **10**(2), 34 (2018).
78. Y. Feng et al., "High-performance and stable perovskite solar cells based on dopant-free arylamine-substituted copper (II) phthalocyanine hole-transporting materials," *Adv. Energy Mater.* **9**, 1901019 (2019).
79. M. Islam et al., "NiO_x hole transport layer for perovskite solar cells with improved stability and reproducibility," *ACS Omega* **2**, 2291–2299 (2017).
80. P. Qin et al., "Copper-doped chromium oxide hole-transporting layer for perovskite solar cells: interface engineering and performance improvement," *Adv. Mater. Interfaces* **3**, 1500799 (2016).
81. J. H. Kim et al., "High-performance and environmentally stable planar heterojunction perovskite solar cells based on a solution-processed copper-doped nickel oxide hole-transporting layer," *Adv. Mater.* **27**(4), 695–701 (2015).
82. H. Zhang et al., "Low-temperature solution-processed $CuCrO_2$ hole-transporting layer for efficient and photostable perovskite solar cells," *Adv. Energy Mater.* **8**(13), 1702762 (2018).
83. J.-S. Yeo et al., "Highly efficient and stable planar perovskite solar cells with reduced graphene oxide nanosheets as electrode interlayer," *Nano Energy* **12**, 96–104 (2015).
84. Q.-D. Yang et al., "Graphene oxide as an efficient hole-transporting material for high-performance perovskite solar cells with enhanced stability," *J. Mater. Chem. A* **5**(20), 9852–9858 (2017).
85. F. Hou et al., "Efficient and stable planar heterojunction perovskite solar cells with an MoO_3/PEDOT:PSS hole transporting layer," *Nanoscale* **7**(21), 9427–9432 (2015).
86. D. Y. Lee, S. I. Na, and S. S. Kim, "Graphene oxide/PEDOT:PSS composite hole transport layer for efficient and stable planar heterojunction perovskite solar cells," *Nanoscale* **8**(3), 1513–1522 (2016).
87. J. M. Wang et al., "Small molecule-polymer composite hole-transporting layer for highly efficient and stable perovskite solar cells," *ACS Appl. Mater Interfaces* **9**(15), 13240–13246 (2017).
88. W.-D. Hu et al., "Copper iodide-PEDOT:PSS double hole transport layers for improved efficiency and stability in perovskite solar cells," *J. Photochem. Photobiol. A* **357**, 36–40 (2018).
89. Q. Luo et al., "Iodide-reduced graphene oxide with dopant-free spiro-OMeTAD for ambient stable and high-efficiency perovskite solar cells," *J. Mater. Chem. A* **3**(31), 15996–16004 (2015).
90. G. W. Kim et al., "Gradated mixed hole transport layer in a perovskite solar cell: improving moisture stability and efficiency," *ACS Appl. Mater. Interfaces* **9**(33), 27720–27726 (2017).

Biographies of the authors are not available.